Fabrication and Characterisation of Metal-Doped Pectin Films

I. Kalathaki[a], K. Alba[a], H. Muhamedsalih[b], and V. Kontogiorgos[a]*

[a] *Department of Biological Sciences, University of Huddersfield, HD1 3DH, UK*
[b] *EPSRC Future Metrology Hub, University of Huddersfield, Huddersfield, HD1 3DH, UK*

*Corresponding author email: v.kontogiorgos@hud.ac.uk

Abstract

Metal-doped pectin films have been fabricated and their thermal, mechanical and microstructural properties were examined by means of complementary physicochemical techniques. Films were fabricated at two pH values, 2.0 and 7.0, with inclusions of metals (Na^+, K^+, Ca^{2+}, Mg^{2+} and Al^{3+}) and conditioned in a range of relative humidity environments. Glass transition temperatures (T_g) of water-plasticised films ranged between 54-95 ^oC. Treatment of T_g values with Gordon-Taylor empirical model revealed a spectacular increase (~25 ^oC) of the T_g of dry films at pH 2.0 and with the addition of metals. Uniaxial extension measurements revealed that, at pH 2.0, films were stronger with lower extensibility in contrast to their counterparts prepared at pH 7.0. All films were microstructurally inspected and revealed a continuous one-phase microstructure at length scales >100 μm with no significant differences in the surface topography. Changes of the physical properties of films have been attributed to the modulation of the intermolecular interactions that are influenced by the degree of ionisation of carboxyl groups (pH), electrostatic interactions (inclusion of cations), and conformational reorientation of pectin chains. Overall, it has been shown that it is possible to engineer biopolymer films for a range of applications depending on the desired operating environment.

Keywords: pectin; biomaterial; film; glass transition; microstructure

1. Introduction

Biopolymer films are amorphous structures that are most frequently formed after condensation of concentrated biopolymer solutions. During solvent evaporation, the constituting biopolymers progressively reduce their molecular mobility resulting in a solid-state amorphous matrix (usually >85% solids). Biopolymer films are often fabricated with polysaccharides, proteins or their blends with addition of various plasticisers or cross-linkers (Vieira, da Silva, dos Santos, & Beppu, 2011) and have a wide range of applications in biomedical, food, and pharmaceutical areas (Rinaudo, 2007). Biopolymer-based films have advantages for certain applications such as biomimetism or biodegradability, nevertheless, they are accompanied by certain drawbacks that are related to their sensitivity to environmental conditions (e.g., moisture) or anisotropy (e.g., in mechanical properties) (Crouzier, Boudou, & Picart, 2010).

Polysaccharides may be relatively simple consisting of one sugar residue (e.g., glucose) lacking tuning capacity of their physical properties without severe chemical functionalisation (e.g., starch). Others are complex biopolymers that are readily influenced by solvent composition (i.e., solvent-polymer interactions), as they already carry functional groups (e.g., carboxyl, methyl, or sulphate), side chains, or various sugar residues (e.g., xanthan or alginates). Pectin is a highly complex heteropolysaccharide that in its simplest description consists of two major blocks, that is homogalacturonan (HG) and rhamnogalacturonan-I (RG-I). HG is a linearly α-(1→4) linked D-galacturonic acid (D-GalA) polymer with methyl-esterified carboxyl groups at the *C*-6 position with the structure becoming increasingly more complex with acetylation at *O*-2 or *O*-3 positions (Mohnen, 2008). The extent of methyl-esterification is termed degree of methylesterification (DM) and for DM < 50% pectin is classified as low methylated (LM) whereas for DM > 50% as high methylated (HM). This distinction is important, as it signals differences in the functional properties of pectins such as gelation or interactions with other species that may be present in the solution (e.g., cations, charged molecules etc.).

Pectin films are diverse biomaterials used in food (Espitia, Du, Avena-Bustillos, Soares, & McHugh, 2014), bioengineering (Di Giacomo, Bonanomi, Costanza, Maresca, & Daraio, 2017), biomedical (Noreen et al., 2017), or drug delivery (Laurén et al., 2018) applications, just to name a few. Reinforcing the microstructure of pectin films with nanoparticles (Makaremi et al., 2017) or micro-particles (Cataldo, Cavallaro, Lazzara, Milioto, & Parisi, 2017) result in composite films with enhanced physical properties. For instance, inclusion of halloysite nanotubes, which is an aluminosilicate mineral (Biddeci et al., 2016; Makaremi et al., 2017), or layered double hydroxide (a clay containing aluminium and magnesium) (Lins, Bugatti, Livi, & Gorrasi, 2018) enhances the mechanical and thermal performance of pectin composite-films. However, the specific role of aluminium or magnesium cations on their physicochemical behaviour has not yet been elucidated. Despite the fact that there is work dedicated to applications of pectin films there is a gap in our understanding on how molecular interactions affect film formation and ultimately its functionality. For instance, modulation of intermolecular interactions of pectin could be a route to manipulate their physico-chemical responses. Indeed, molecular interactions of pectin chains have been explored in our previous investigations where we were able to modulate the stability of pectin-stabilised emulsions (Alba, Sagis, & Kontogiorgos, 2016; Kpodo et al., 2018) and its solution conformation (Alba, Bingham, Gunning, Wilde, & Kontogiorgos, 2018) by tuning its molecular architecture.

This naturally led us to formulate our current hypothesis that by modulating the macromolecular interactions of pectin chains in the liquid state we would be able to control the physical properties of the films in the solid-state. Consequently, the objectives of the present work were to fabricate pectin films with a spectrum of physical properties and characterise them so as to understand and ultimately predict their physicochemical behaviour.

2. Materials and Methods

2.1 Materials

Unstandardized citrus HM-pectin (GENU Pectin Type B Rapid Set-Z) was obtained from CP Kelco (UK). All salts and D-sorbitol that were used to fabricate the films (NaCl, KCl, $CaCl_2$, $MgCl_2$, $AlCl_3$) and to create atmospheres of constant relative humidity (P_2O_5, LiCl, $MgCl_2$, $Mg(NO_3)_2$) were purchased from Sigma-Aldrich (Poole, UK) and were of analytical grade. Sodium azide 0.02 g dL^{-1} was used as a preservative in all samples.

2.2 Molecular characterisation of pectin

Molecular characteristics (M_w, M_n, and R_g) of pectin samples were determined by means of size exclusion chromatography coupled to a multi-angle light scattering detector (SEC-MALS), as described in detail in our previous investigation (Kpodo et al., 2017). For intrinsic viscosity measurements, pectin (0.01-1 g dL^{-1}) and salts were dispersed in distilled water and left overnight under continuous stirring at room temperature until complete solubilisation. The ionic strength of all salt solutions was kept at 100 mM and the pH was adjusted with the aid of 100 mM HCl or NaOH to 2.0 or 7.0, respectively. Intrinsic viscosity was determined using a Ubbelohde capillary viscometer at 20 ^oC with the aid of Huggins and Kraemer equations. Steady shear rheological measurements were carried out at 20 ^oC using a Bohlin Gemini 200HR Nano Rotational rheometer (Malvern Instruments, Malvern, UK) equipped with a double gap geometry (DG 24/27) and all measurements were implemented in steady shear mode in the range between 1-1000 s^{-1}. Apparent degree of methylesterification (DM) of films was measured before conditioning by a Fourier transform infrared spectrometer (FT-IR, Thermo Nicolet 380, Thermo Scientific, UK) in the range of 400-4000 cm^{-1}. Commercial pectins (CP Kelco, UK) with known DM were used to construct a calibration curve to determine the DM of the samples from the area of peaks between 1730 and 1720 cm^{-1} (methyl esterified groups) and 1630 and 1600 cm^{-1} (carboxylate anion) as $DM = A_{1730}/(A_{1730}+A_{1630})$ (Chatjigakis et al., 1998).

142 *2.3 Film preparation*

143 Pectin (4 g dL^{-1}) was dispersed at room temperature in distilled water and pH was adjusted to
144 either 2.0 or 7.0 with the aid of 100 mM HCl or NaOH. Metal doping was performed at the same
145 ionic strength (100 mM) for all salts (NaCl, KCl, $CaCl_2$, $MgCl_2$, $AlCl_3$). Sorbitol (5 g dL^{-1}) was
146 added as plasticiser only in films that were used for tensile measurements. For the latter samples,
147 this process yields films with composition of ~45% pectin and ~55% sorbitol in dry matter. Salts
148 were added in the pectin dispersions and after overnight solubilisation the solutions were centrifuged
149 for 5 min at 4000 g to ensure the removal of air bubbles. Solutions were cast (~100 mL) in ~240
150 cm^2 teflon-coated pans and left to dry at room temperature for ~7 days. Following drying, films
151 were manually peeled out of the pan with the fabrication process yielding samples with average
152 thickness of 250 μm. Before any analysis, the dried films were cut to shape and conditioned in
153 desiccators under different relative humidities at room temperature with the aid of super-saturated
154 salt solutions (P_2O_5, LiCl, $MgCl_2$, and $Mg(NO_3)_2$ for %RH of 0.0, 11.1, 33.3, 53.6 at 20 ^oC,
155 respectively). Samples were conditioned until no measurable changes in moisture content could be
156 detected (~10-30 days). Films with sorbitol were handled in the same manner as the water-
157 plasticized specimens.

158

159 *2.4 Thermal Analysis*

160 Moisture content determination was carried out by thermogravimetric analysis with a TGA1
161 system (TGA, Mettler-Toledo, UK) on ~15 mg samples. The samples were weighed into alumina
162 crucibles and heated at 10 °C min^{-1} from 30 °C to 200 °C under nitrogen flow (50 ml min^{-1}) for both
163 the balance and the sample crucible. Moisture content was calculated from the weight losses
164 between 30-150 °C (Nisar et al., 2018). To determine the glass transition temperatures (T_g) of the
165 films, differential scanning calorimetry (DSC) experiments were carried out on ~30 mg samples
166 using a DSC1 calorimeter (Mettler-Toledo, UK). Conditioned samples were weighed into a 40 μl
167 aluminium pans and were hermetically sealed. Samples were heated under nitrogen flow (50 ml

168 min^{-1}) using an empty pan as a reference into two stages so as to erase thermal history with the
169 following protocol: heated at 10 °C min^{-1} from -20 - 90 °C, quenched cooled to -20 °C, and heated
170 at 10 °C min^{-1} from -20 °C to 90 °C. Temperature calibrations were carried out with indium while
171 the heat capacity was calibrated with sapphire. Glass transition temperatures were obtained from
172 the peaks of the first derivative of heat flow of the first scan that corresponds to the middle point of
173 the transition of the heat flow curve. To construct state diagrams, experimental data of T_g were fitted
174 to the empirical Gordon–Taylor equation using Prism (Graphpad Software, San Diego, USA):

175 $$T_g = \frac{w_1 T_{g_1} + k w_2 T_{g_2}}{w_1 + k w_2}$$

176 where w_1 and w_2 are the respective weight fractions of the pectin and water, T_{g1} is the T_g of the dry
177 biopolymer, T_{g2} is the T_g of pure water (-138 °C, 135 K), and k is a constant related to the strength
178 of polymer-diluent interaction (the larger the k the greater the plasticisation effect) (Biliaderis,
179 Lazaridou, & Arvanitoyannis, 1999). Measurements were performed in triplicate and thermal traces
180 were collected and analysed using the STARe software (Mettler-Toledo, UK).
181
182 *2.5 Tensile measurements*
183 Films were cut to specific dimensions in a "dog bone" shape (40 x 8 mm) (American Society
184 for Testing and Material at Standard Designation D882-02) and conditioned in the desiccator with
185 52% relative humidity ($Mg(NO_3)_2$). The thickness of each specimen was measured with a
186 micrometre at three points along its length (average thickness of 250 μm). Tensile measurements
187 were carried out on a TA-XT2i instrument (Stable Micro Systems Ltd, Surrey, UK) equipped with
188 tensile grips (A/TG model) in ten replicates for each condition at an extension rate of 1 mm/sec.
189 Tensile strength was calculated by dividing the maximum load by the cross-sectional area of the
190 film and toughness was calculated by determining the area under the stress-strain curves. Young
191 modulus was evaluated as the gradient of stress-strain curves at low deformations, whereas Hencky
192 strain (ε_h) was calculated as $\varepsilon_h = ln(L/L_o)$ with L being the elongated and L_o the initial lengths of the
193 specimens.

194 *2.6. Surface topography analysis*

195 Scanning electron microscopy (SEM) and white-light coherence scanning interferometer
196 (CSI) were employed for inspecting and measuring the surface texture of the films. SEM was carried
197 out on films using an FEI Quanta FEG 250 (ThermoFischer Scientific, USA) scanning electron
198 microscope with a high vacuum mode. Samples were fixed to a 50 mm diameter aluminium stub
199 plate using Agar Scientific adhesive conductive-carbon sheet. The samples were sputter coated
200 (Quorum Technology SC7920), with a thin layer of Au/Pd for a time period of 60 sec, prior to
201 examination. The images were captured at 10 kV accelerating voltage using the back scattered
202 electron detector to produce a back scattered electron image. CSI (Ametek Taylor-Hobson, UK)
203 was used to provide quantitative surface measurements with a 0.1 nm axial resolution and 0.8 μm
204 lateral resolution using 20x objective lens. Samples were aligned within the objective depth of focus
205 before scanning the interferometer across the sample surface. Three measurements across each
206 sample were carried out to enhance the measurement accuracy. The field-of-view of a single
207 measurement was set at 0.918x0.918 mm. Each measurement was processed before extracting the
208 root mean square height roughness parameter (*Sq*) by levelling the surface *via* a second order
209 polynomial fitting and filtering the waviness components *via* a Gaussian robust filter with cut-off
210 wavelength equal to 0.25 mm.

211

212 **3. Results and Discussion**

213 *3.1 Characterisation and solution behaviour of pectin*

214

215 Weight-average (M_w, 183 x10^3 g mol^{-1}) and number-average (M_n, 119 x10^3 g mol^{-1}) molecular
216 weights, polydispersity index (M_w/M_n, 1.5) and radius of gyration (R_g, 43 nm) of pectin that was
217 used in film preparation were determined by size exclusion chromatography. Molecular weight and
218 its distribution has a profound effect on the physical properties in both polysaccharide, as for
219 example in pullulan (Lazaridou, Biliaderis, & Kontogiorgos, 2003) or chitosan, (Hwang, Kim, Jung,
220 Cho, & Park, 2003) and synthetic polymer (Perron & Lederman, 1972) films. Generally, high

molecular weight chains result in stronger films compared to their low molecular weight counterparts because short chains increase molecular mobility resulting in samples with lower glass transition temperatures, tensile strength, and elastic modulus (Sperling, 2006). Polydispersity index of pectin sample revealed relatively narrow molecular weight distribution indicating that the contribution of large polymer chains is only to a limited extent greater than those of small molecular weight. Consequently, it will be difficult to ascribe any observed differences in the physical properties of the films exclusively to the molecular weight distribution of the initial material (i.e., polydispersity). Rather, degree of methylesterification and conformational changes induced by pH and inclusion of cations are expected to play greater role, as they will act cooperatively to affect the efficiency of chain packing (Alba et al., 2018) thus influencing the free volume and molecular mobility of the condensed systems.

Naturally, the next step would be to identify solution conformational changes that may be induced by modifications of solvent quality in the liquid state, as the first stage in film preparation involves dispersion of pectin into the appropriate cation-containing solution. Intrinsic viscosity measurements, which reflect the hydrodynamic volume of isolated pectin chains and give first insights to their conformational status, is not particularly influenced by the presence of different metals or pH (Table 1). This behaviour is in accordance with our recent studies where solution conformation of high DM pectins, as the one we used in the present investigation, are not affected by changes in pH (Alba et al., 2018). This occurs because pectins with high DM (> ~50) are not influenced considerably by electrostatic interactions because of their low charge density in contrast to low DM pectins (< ~30). As a causal consequence, the effect of chain interactions with metals in solution will also be minimal. Indeed, the effect of cations on intrinsic viscosity becomes evident only at pH 7 for the multivalent metals that have the ability to form cross-links between the carboxyl groups of pectin chains resulting in formation of water-insoluble aggregates (Li, Al-Assaf, Fang, & Phillips, 2013). This limiting behaviour was further demonstrated by the trivalent Al^{3+} that at pH 7 did not form solutions at all and consequently films, as the samples gelled due to chain cross linking

during preparation. It should be mentioned that aggregate formation and gelation critically depends on the ion concentration as well as the fine structure of pectin.

Table 1. Intrinsic viscosity ([η]), critical concentration (c^*), and coil overlap parameter ($c^*[\eta]$) of citrus pectin at different pH and metal content.

		[η] (dL g^{-1})	c^* (g dL^{-1})	$c^*[\eta]$
pH 2	No salt	3.45	0.25	0.9
	NaCl	3.29	0.23	0.8
	KCl	3.38	0.20	0.7
	$CaCl_2$	3.03	0.20	0.6
	$MgCl_2$	2.95	0.21	0.6
	$AlCl_3$	3.29	0.24	0.8
pH 7	No salt	3.47	0.25	0.9
	NaCl	3.41	0.27	0.9
	KCl	3.84	0.23	0.9
	$CaCl_2$	2.31	0.11	0.2
	$MgCl_2$	2.46	0.14	0.3

It is possible to calculate the critical biopolymer concentration, c^*, with construction of double logarithmic plots of zero shear specific viscosity ($(\eta_{sp})_o$) against reduced concentration ($c[\eta]$) (Figure S1). This approach evaluates the influence of solvent environment on pectin interactions, as concentration increases away from the dilute region and approaches the semi-dilute regime. In agreement with intrinsic viscosity trends, critical concentration is essentially constant for all except the two samples containing Ca^{2+} and Mg^{2+}. In addition, the total volume occupied by the chains at the critical concentration, c^*, as expressed by the dimensionless coil overlap parameter ($c^*[\eta]$), begins to decrease for these two samples at pH 7 indicating lower volumes due to cross linking (Table 1).

We have established, so far, that pH and addition of cations exerts limited influence on the hydrodynamic characteristics of pectin chains and, therefore, film formation will essentially commence from pectin solutions with similar hydrodynamic volumes. However, conformational changes may still be induced by drying and differences in the physical properties of the solid-state systems (e.g., thermal or mechanical) could be attributed not only to the alteration in the strength of

the interactions but also to conformational changes of pectin, as systems transition from the liquid to the glassy state.

3.2 Spectroscopic analysis and thermal properties

The first step was to investigate how film-forming conditions influence the DM of pectin, as it is one of the most important parameters that governs pectin functionality (Figure 1, Table 2). Peaks at 1620 cm^{-1} of FT-IR spectra originate form stretching vibrations of carboxylate anions (COO^-) and those at around 1730 cm^{-1} from carbonyl of methyl-esterified and carboxyl groups (COOH). The area under these peaks plays central role in pectin analysis, as is possible to determine the apparent DM of the samples (Table 2) (Chatjigakis et al., 1998).

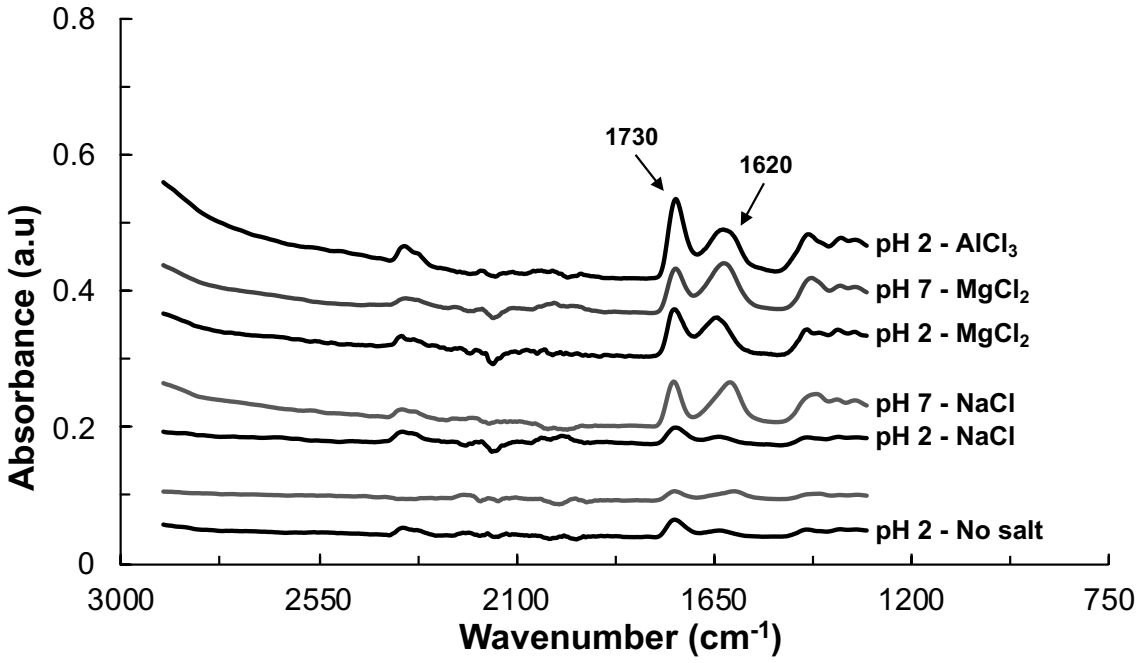

Figure 1: FT-IR spectra of representative pectin films at pH 7.0 and 2.0. Area under the peaks at around 1730 and 1620 cm^{-1} was used to estimate an apparent degree of methylesterification.

288 **Table 2.** Apparent degree of methylesterification of pectin films.

Samples		Apparent DM (%)
Pectin powder		79 ±1.1[a]
pH 2	No salt	79 ±1.7[a]
	NaCl	74 ±1.0[a]
	KCl	75 ±2.2[a]
	$CaCl_2$	62 ±7.8[b]
	$MgCl_2$	59 ±1.7[b]
	$AlCl_3$	61 ±1.0[b]
pH 7	No salt	51 ±5.2[c]
	NaCl	45 ±1.1[c,d]
	KCl	49 ±6.7[c]
	$CaCl_2$	45 ±2.8[c,d]
	$MgCl_2$	40 ±1.3[d]

289 *Means that do not share a letter are significantly different.
290

291 The distinct influence of pH on the apparent DM is evident irrespectively of the specimen. In
292 particular, fabrication of films at pH 7 results in a decrease of apparent DM. As the technique is
293 sensitive to the ionisation state of the carboxyl group (Fellah, Anjukandi, Waterland, & Williams,
294 2009), at pH values above ~3.5 the amount of COO^- increases due to the dissociation of COOH thus
295 affecting the area under the curve and DM appears to decrease. Limited pectin demethylation during
296 sample solubilisation, film formation (i.e., dehydration), and conditioning stage (Einhorn-Stoll,
297 Benthin, Zimathies, Görke, & Drusch, 2015) by means of β-elimination reactions and saponification
298 that may occur in pectins at pH > 6.0 (Diaz, Anthon, & Barrett, 2007; Einhorn-Stoll, Kastner,
299 Urbisch, Kroh, & Drusch, 2018) may also offer another plausible explanation for the decrease of
300 DM values. This reaction is further facilitated in high DM pectins, as methoxyl groups attached to
301 a galacturonic acid are particularly labile. Cations did not seem to have strong influence on apparent
302 DM and only a marginal reduction in apparent DM with increase of valency was observed at pH 2.0
303 (Table 2.0). It should be mentioned that limited acid hydrolysis (occurring at pH 2.0) and β-
304 elimination (occurring at pH 7.0) during sample preparation could contribute to molecular weight
305 reduction of the initial material although the extend of this degradation was not assessed in the
306 present study. Consequently, findings reveal that fabrication of pectin films, irrespectively of how
307 it proceeds, may result in permanent structural changes in the molecular architecture of pectin that

may influence vitrification events and film functionality. For instance, demethylation may assist interactions with water or enhance cross linking with multivalent cations through the exposed carboxyl groups whereas extensive acid hydrolysis may result in increased molecular mobility of the chains in the amorphous state.

Glass transition temperatures (T_g) of water plasticised metal-doped pectin films in the absence of sorbitol were investigated by differential scanning calorimetry (DSC) (Figure 2) and moisture content was determined by thermogravimetric analysis (Figure S2). The glass transitions are usually obtained from thermograms of the second scan immediately after quenching to erase thermal history of the samples. However, this experimental approach resulted in weak thermal events and the peaks of the first derivatives of the heat flow from the first run were used instead to identify the midpoint of glass transitions (Figure 2, inset). It should be noted that fast transitions to the out-of-equilibrium state (i.e., fast water evaporation, in the present study) result in films with greater enthalpic content

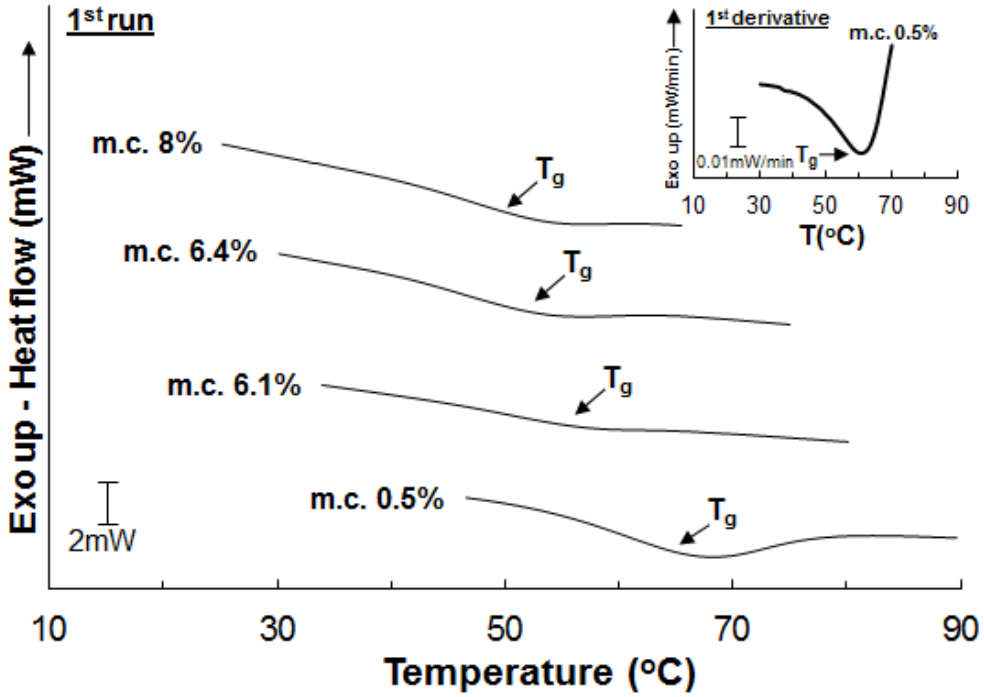

Figure 2: Typical DSC thermograms for pectin films at different moisture contents (m.c). Arrows indicate the position of the midpoint of the glass transition that was obtained from the peak of the first derivative of heat flow (inset).

than those formed *via* slow processes (Angell, 1995). However, since the dependence of T_g on the rate of glass formation is weak, T_g becomes a material characteristic (Debenedetti & Stillinger,

2001) and minor discrepancies in the rate of film formation does not affect comparisons of thermal behaviour between the samples.

Thermal traces of films revealed one endothermic transition between ~55-95 ^{o}C depending on the moisture content of the sample. Increase of moisture shifts glass transition to lower temperatures, which is typical because of the water-plasticisation effect on films (Figure 2) (Biliaderis et al., 1999; Lazaridou & Biliaderis, 2002; Lazaridou et al., 2003). The endothermic event that was identified in the first run frequently includes enthalpic relaxations due to sub-T_g local rotational and vibrational motions that do not cease to exist after glass formation, especially in samples stored relatively near their glass transition temperature. This thermal event was not dominant, yet it was further diminished in the second scan, which gives strong evidence that glass reorganisation takes place in pectin films, albeit slowly, during conditioning at room temperature. This type of thermal relaxation occurs as pectin chains attempt to reach equilibrium through sub-T_g motions of side chains (e.g., of the RG-I segments), methyl ester rotations of the D-GalA or even due to the flexibility that is imparted to the whole chain because of the presence of rhamnose residues (Axelos & Thibault, 1991). These motions result in physical ageing of the specimens and may have ramifications for the mechanical properties of the films (Hutchinson, 1995).

Glass transition temperatures collected from the previous step were fitted to the empirical Gordon-Taylor (GT) model to construct state diagrams of the films (Figure 3). This approach allows following the moisture-content depression of T_g and obtain information on the influence of pH and metals on the glass transitions of the films. GT-modelling enables calculation of the glass transition of the dry polymer (T_{g1}) and constant k that indicates the plasticisation effect of water, with higher k values indicating higher plasticisation efficiency (Table 3).

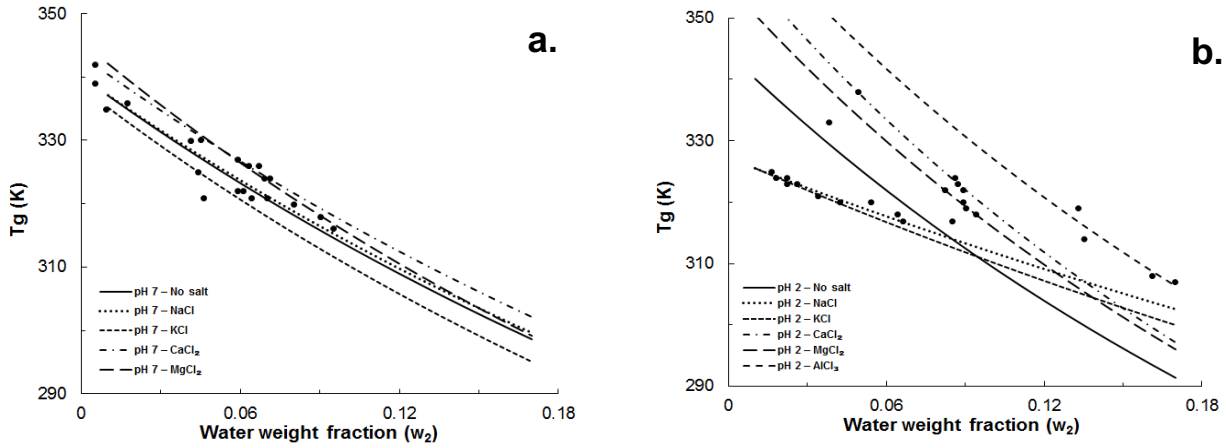

Figure 3: State diagrams of metal-doped pectin films at a) pH 7.0 and b) pH 2.0. Lines represent the G-T fitting of the experimental data (solid dots).

Table 3: Parameters of the GT equation using T_g data from DSC measurements.

Samples		T_{g1} (K)	k	r^2
pH 2	No salt	344	1.8	0.74
	NaCl	327	0.8	0.98
	KCl	328	0.9	0.97
	$CaCl_2$	361	2.1	0.99
	$MgCl_2$	355	2.0	0.97
	$AlCl_3$	368	1.9	0.89
pH 7	No salt	340	1.3	0.98
	NaCl	340	1.3	0.96
	KCl	338	1.4	0.74
	$CaCl_2$	344	1.3	0.99
	$MgCl_2$	346	1.5	0.96

Irrespectively of the treatment, samples prepared at pH 7.0 present lower T_{g1} values than those at pH 2.0. This behaviour is attributed to the influence of pH on pectin conformation in solution before vitrification takes place. Pectins with high degree of methylesterification at low pH exhibit low correlation lengths and high fractal dimensions resulting in "dense" structures in contrast to pH 7.0 that have lower capacity to fill space efficiently ("open" structures) with hydrogen bonding being

368 the major molecular driving force (Alba et al., 2018; Li et al., 2013; Yoo, Fishman, Hotchkiss, &
369 Lee, 2006). In addition to intermolecular hydrogen bonding, degree of blockiness has been also
370 shown to control structure formation and strength of pectin gels (Ström et al., 2007) albeit this
371 parameter was not quantified in our sample. Pectin chains may also undergo conformational changes
372 attaining two-folded (2^1) or three folded (3^1) helical structures (Morris, Powell, Gidley, & Rees,
373 1982). Both types of conformations are equally favoured and depending on the solvent environment
374 one or another form may be prevalent (Braccini, Grasso, & Pérez, 1999). Generally, at high pH the
375 2^1 conformation is favoured but at low pH and in the solid state (Morris et al., 1982) the 3^1 is
376 preferred that may also result in denser packing of the chains. This state of affairs creates lower free
377 volume and molecular mobility for the films fabricated at pH 2.0 thus yielding higher glass transition
378 temperatures. As discussed above, limited demethylation of pectin at pH 7.0 and conversion to its
379 low-methoxylated counterpart may also play a role, as it has been already rheologically shown that
380 in high solid systems of LM-pectins tuning pH to neutral influences free volume resulting in early
381 vitrification compared to systems at low pH (Alba, Kasapis, & Kontogiorgos, 2015).

382 Glass transition temperatures of the dry polymer remain essentially unaffected with inclusion
383 of doping metals at pH 7.0 ranging between 340-346 ^{o}K (67-73 ^{o}C). It appears that chain interactions
384 are not particularly influenced by the presence of metals resulting in glasses with similar free volume
385 and minimal changes in the T_{g1} of the specimens (~ 5 ^{o}C, Table 3, Figure 3a). However, the other
386 extreme of pectin ionisation (pH 2.0) brings about the most spectacular manipulation in the thermal
387 properties of the films resulting in a progressive increase of T_{g1} of up to ~25 ^{o}C compared to the
388 control samples (Table 3, Figure 3b). The monovalent cations showed a tendency to decrease T_{g1}
389 whereas bivalent and trivalent cations progressively increase its value. This behaviour is attributed
390 to the interaction strength of cations with water and HG segments of pectin chains (Huynh, Lerbret,
391 Neiers, Chambin, & Assifaoui, 2016). In particular, Mg^{2+} interacts strongly with water and it
392 remains weakly bound to HG segments being unable to form cross-links between pectin chains
393 with only polycondensation occurring. In contrast Ca^{2+} forms transient ionic cross-links with poly-

394 galacturonic acid chains (Huynh et al., 2016) resulting in stiffer chain-pairs with lower molecular
395 mobility and higher T_{g1} something that is clearly observed at pH 2 even though chain ionisation at
396 this pH is limited. In the same manner, Al^{3+} cations that have the tendency to interact even stronger
397 than Ca^{2+} with pectin chains (Franco, Chagas, & Jorge, 2002) result in even lower molecular
398 mobility and higher T_{g1}. In contrast, monovalent cations (Na^{+}, K^{+}) play little role on pectin
399 conformation, as they are not involved in order-disorder transitions or cross-linking (Cescutti &
400 Rizzo, 2001) and their influence is limited to the screening of electrostatic interactions and
401 competition with pectin for water resulting in a decrease of T_{g1} of about 17 ^{o}C. Finally, water
402 appears to be more efficient plasticiser at low pH, as reflected in the parameter *k*. Generally, the
403 higher *k* values that are observed at pH 2 signify that small increments of moisture content results
404 in large T_g depression. This may be influential in film functionality where moisture is the dominant
405 element of the operating environment (e.g., wound dressing or food packaging), as they will be
406 sensitive to moisture uptake. We have shown that macromolecular interactions between pectin
407 chains can be tuned to modulate the thermal properties of the films. Since continuum physical
408 properties of polymeric materials such as their mechanical behaviour are inherently connected to
409 glass transition temperature, the next step was to probe the tensile and microstructural properties of
410 the films that are described in the next section
411
412 *3.3 Tensile measurements and film microstructure*
413
414 Uniaxial deformation measurements were carried out on selected samples in the presence of
415 sorbitol (5 g dL^{-1}) to facilitate handling of films (Figure 4). Inclusion of polyols in biopolymer films,
416 reduces the energy required for molecular motion with the formation of hydrogen

bonds between hydroxyl groups of monosaccharide residues of the chains and polyol. As a result, the introduction of polyols in the unoccupied spaces between biopolymer chains increases free volume and molecular mobility with concomitant depression of T_g (Vieira et al., 2011).

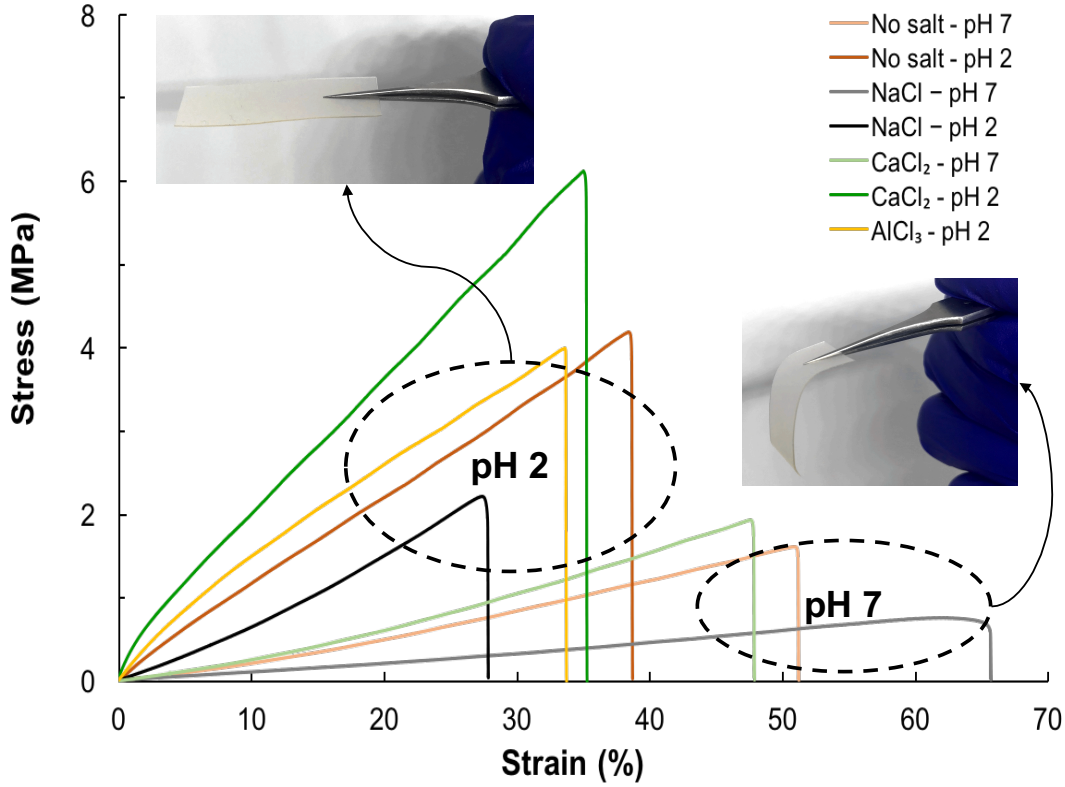

Figure 4: Stress-strain curves of metal-doped pectin films at pH 2.0 and 7.0. Samples at pH 2.0 tend to be stiffer (top left inset) with higher tensile strengths than those at pH 7.0 (bottom right inset).

However, the aforementioned mechanism of action occurs without influencing electrostatic interactions that are modulated by changes of pH or addition of cations. Consequently, the presence of sorbitol is not expected to have a measurable influence on the fundamental modes of macromolecular interactions between the chains that were described in the previous section. Although T_g was not measured and modelled for the samples with sorbitol the overall trends in the mechanical behaviour is in agreement with the thermal properties that were discussed in the previous section.

Initial inspection of the plots reveals the clear influence of pH on the mechanical properties, as films fabricated at pH 7 result in specimens with significantly lower tensile strengths and Young moduli, and higher Hencky strains than those at pH 2, irrespectively of the cation that was used

433 (Table 4). Moisture content, which is one of the major determinants of elasticity in biopolymer
434 films, ranged between 8-17 % (Table 4) and could potentially account for the observed differences.
435 Closer examination of the curves (Figure 4) and Table 4 reveals that there is no relationship between
436 moisture content and tensile properties of the films. For example, despite the fact that samples with
437 Al^{3+} contained the highest moisture content they exhibited particularly high tensile strength and
438 Young modulus whereas samples with sodium at pH 7.0 containing lower water content showed
439 higher extensibility. Such anomalous behaviour of water plasticisation has been previously observed
440 in biopolymer films and has been attributed to reorganisation of the amorphous state and free
441 volume changes during film conditioning (Lazaridou & Biliaderis, 2002; Lazaridou et al., 2003). In
442 addition, control and $CaCl_2$ samples had similar moisture content, at both pH 7.0 and pH 2.0,
443 showing clearly that pH and not the plasticizing effect of water is the predominant factor affecting
444 the tensile properties of the films. Consequently, water content is not the determinant factor and
445 intermolecular interactions controlled by pH between pectin chains appear to be the primary factor
446 that influence the mechanical properties of the samples. Furthermore, the stress *vs.* strain curves
447 show a linear trend for all the investigated films indicating that the transition from the elastic to
448 plastic region was not detected even after the breaking of the specimens. Consequently, the films
449 behave elastically until their breaking point and their deformations are always reversible.
450 Calculation of the area under the stress-strain curves provide first insights to the energy that is
451 reversibly stored in the films during the test and is frequently termed "toughness" (Table 4). Samples
452 at pH 2.0 are generally significantly tougher than their counterparts at pH 7.0, with the exception of
453 samples containing sodium, showing that it is possible to create materials with a range of responses
454 with modification of electrostatic interactions.
455
456
457

458 **Table 4:** Moisture content**,** tensile strength, Young's modulus, toughness, Hencky strain, and root
459 mean square height roughness parameter (*Sq*) values of selected pectin films. Means that do not
460 share a letter are significantly different at $p < 0.05$.
461

		Water (%)	Tensile strength (MPa)	Young's modulus (MPa)	Toughness (N.mm)	Hencky strain (ε_h)	*Sq* (μm)
pH 2	No salt	12.4 ± 0.5^{b}	4.3 ± 1.1^{a}	11.5 ± 2.9	72 ± 21^{a}	0.32 ± 0.05^{abc}	0.084^{a}
	NaCl	8.4 ± 0.8^{c}	2.7 ± 0.7^{bc}	5.9 ± 0.9^{d}	29 ± 12^{b}	0.25 ± 0.05^{a}	0.088^{a}
	$CaCl_2$	11.8 ± 0.4^{a}	5.8 ± 1.3^{d}	25.3 ± 4.5^{c}	81 ± 32^{a}	0.30 ± 0.04^{ab}	0.108^{a}
	$AlCl_3$	17.6 ± 0.8^{b}	3.8 ± 0.6^{ab}	19 ± 2.5^{b}	57 ± 18^{a}	0.29 ± 0.04^{ab}	0.118^{a}
pH 7	No salt	12 ± 0.3^{a}	2.0 ± 0.9^{c}	2.1 ± 0.6^{a}	34 ± 15^{b}	0.39 ± 0.08^{d}	0.102^{a}
	NaCl	10.9 ± 1.5^{a}	0.8 ± 0.1^{e}	1.2 ± 0.3^{a}	72 ± 21^{b}	0.52 ± 0.09^{d}	0.243^{a}
	$CaCl_2$	11.2 ± 0.5^{a}	2.1 ± 0.5^{c}	2.7 ± 0.4^{a}	35 ± 12^{b}	0.38 ± 0.06^{dbc}	1.473^{b}

462

463 Biopolymer film strength also depends on microstructural defects that may act as focal points
464 for stress proliferation resulting in failure of the specimens. Consequently, the last stage of the
465 investigation was to obtain microstructural information that may give insights on the mechanical
466 behaviour of films and identify structural differences between the samples with changes in the
467 fabrication conditions. Macroscopically all films were optically transparent and objects behind them
468 were visible (e.g., text in Figure 5a, d). In addition, they could be easily distinguished by the pH of
469 formation, as films prepared at pH 7 had an off-yellow hue irrespectively of the cation that was
470 introduced in contrast to their clearer counterparts fabricated at pH 2 (Figure 5a, d).

471

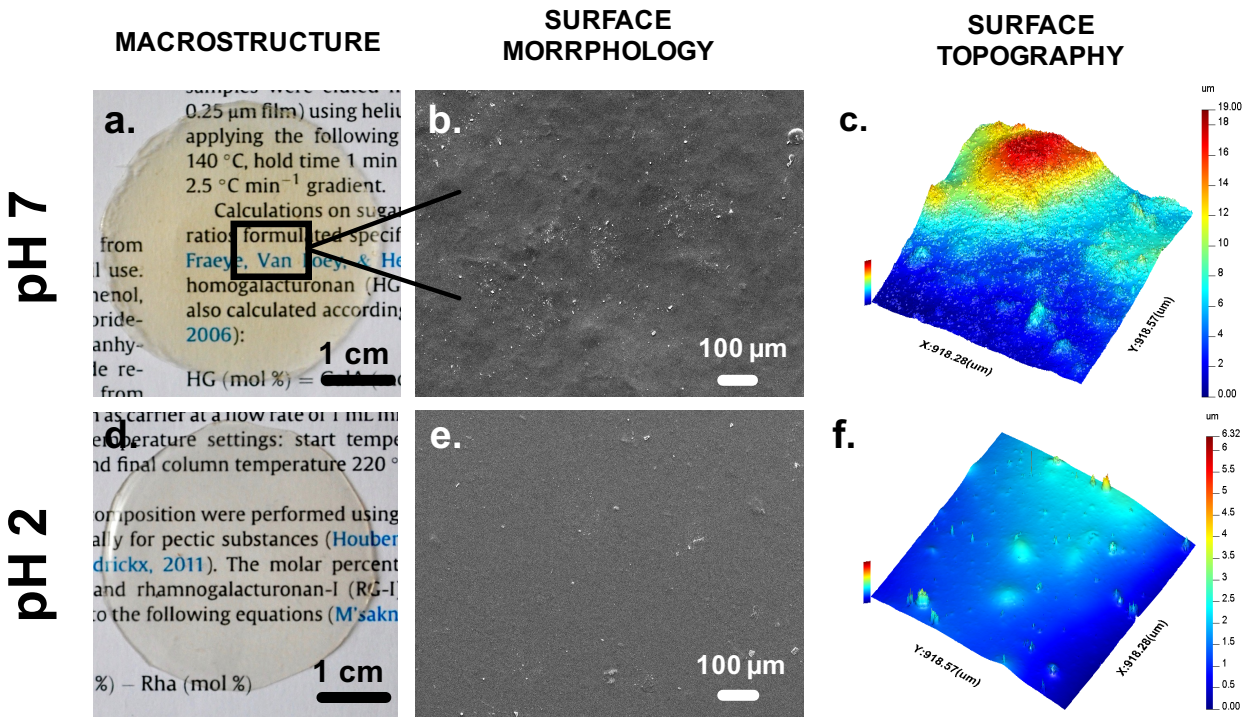

Figure 5: Typical morphological characteristics of metal-doped pectin films at different length scales. (a, b, c) Samples at pH 7 have yellow hue and surfaces with rough morphological and topographical features. (d, e, f) Samples at pH 2 are clear with smoother surfaces. Specimens shown are films doped with $CaCl_2$.

Observations at higher length scales (100 µm) revealed that all films are isotropic one-phase systems with no evident phase separated regions (Figure 5b, e). Such regions could be present either because of plasticiser immiscibility or micro-aggregates of pectin that may be formed during vitrification. Isotropic film formation revealed that differences in the mechanical strength of the specimens could not be attributed to micro-phase separated regions. However, some specimens showed irregular microstructural characteristics (e.g., ripples) or cracks at higher length scales (Figure S3) that may also contribute to the observed differences in the mechanical properties. Since SEM provides only qualitative surface inspection, CSI with the aid of the root mean square height roughness parameter (*Sq*) was employed to measure the surface topography of the films. (Figure 5c, f, Table 4). No significant differences in the *Sq* values between samples were found, except for those fabricated with $CaCl_2$ at pH 7 that presented distinct surface characteristics (Table 4). The surface topography of this sample revealed significant peaks and valleys that affect the local roughness of the sample with the maximum peak height parameter (*Sp*) being 6.65 µm after surface levelling.

Such surface roughness may stem from density fluctuations during the vitrification process thus creating localised distinct "rough" areas in this sample (Figure 5c). On the contrary, the surface topography of the other specimens revealed that the maximum depth of the irregular surfaces is less than 50 nm presenting insignificant impact on the local roughness and consequently on the mechanical properties of the films (Figure S3). Taking everything into account, macromolecular interactions play greater role than surface characteristics for the differences in the mechanical properties of the films and optimisation of the functionality should be focused on tuning the strength and type of interactions.

4. Conclusions

Adjustment of thermophysical properties of pectin films was achieved by manipulation of macromolecular interactions thus confirming our initial hypothesis. The most influential factor that controls the overall physical properties of the films was pH with further fine-tuning being possible by doping with cations of variable valency. In particular, pH 2 and metal inclusion results in a spectacular gradual increase of T_g of up to 25 ^{o}C whereas at pH 7 the effect is muted (~ 5 ^{o}C). This is a result of dense structure formation in solution at low pH prior to vitrification creating lower free volume resulting in higher T_g compared to samples formed at neutral pH. Modulation of forces at the molecular level ultimately results in films with different tensile properties. Those fabricated at pH 2 were substantially stronger exhibiting lower extensibility with the microstructural characteristics playing minimal role in defining mechanical properties. Overall, it has been shown that it is possible by controlling the interplay of the molecular interactions to tailor the physical properties of pectin films and engineer biomaterials for a series of applications.

519 **References**
520

521 Alba, K., Bingham, R. J., Gunning, P. A., Wilde, P. J., & Kontogiorgos, V. (2018). Pectin
522 Conformation in Solution. *The Journal of Physical Chemistry B,* 122, 7286-7294.
523 Alba, K., Kasapis, S., & Kontogiorgos, V. (2015). Influence of pH on mechanical relaxations in
524 high solids LM-pectin preparations. *Carbohydrate Polymers,* 127, 182-188.
525 Alba, K., Sagis, L. M. C., & Kontogiorgos, V. (2016). Engineering of acidic O/W emulsions with
526 pectin. *Colloids and Surfaces B: Biointerfaces,* 145, 301-308.
527 Angell, C. A. (1995). Formation of Glasses from Liquids and Biopolymers. *Science,* 267, 1924.
528 Axelos, M. A. V., & Thibault, J. F. (1991). Influence of the substituents of the carboxyl groups
529 and of the rhamnose content on the solution properties and flexibility of pectins.
530 *International Journal of Biological Macromolecules,* 13, 77-82.
531 Biddeci, G., Cavallaro, G., Di Blasi, F., Lazzara, G., Massaro, M., Milioto, S., . . . Spinelli, G.
532 (2016). Halloysite nanotubes loaded with peppermint essential oil as filler for functional
533 biopolymer film. *Carbohydrate Polymers,* 152, 548-557.
534 Biliaderis, C. G., Lazaridou, A., & Arvanitoyannis, I. (1999). Glass transition and physical
535 properties of polyol-plasticised pullulan–starch blends at low moisture. *Carbohydrate*
536 *Polymers,* 40, 29-47.
537 Braccini, I., Grasso, R. P., & Pérez, S. (1999). Conformational and configurational features of
538 acidic polysaccharides and their interactions with calcium ions: a molecular modeling
539 investigation. *Carbohydrate Research,* 317, 119-130.
540 Cataldo, V. A., Cavallaro, G., Lazzara, G., Milioto, S., & Parisi, F. (2017). Coffee grounds as
541 filler for pectin: Green composites with competitive performances dependent on the UV
542 irradiation. *Carbohydrate Polymers,* 170, 198-205.
543 Cescutti, P., & Rizzo, R. (2001). Divalent Cation Interactions with Oligogalacturonides. *Journal*
544 *of Agricultural and Food Chemistry,* 49, 3262-3267.
545 Chatjigakis, A. K., Pappas, C., N.Proxenia, O.Kalantzi, P.Rodis, & Polissiou, M. (1998). FT-IR
546 spectroscopic determination of the degree of esterification of cell wall pectins from stored
547 peaches and correlation to textural changes. *Carbohydrate Polymers,* 37, 395-408.
548 Crouzier, T., Boudou, T., & Picart, C. (2010). Polysaccharide-based polyelectrolyte multilayers.
549 *Current Opinion in Colloid & Interface Science,* 15, 417-426.
550 Debenedetti, P. G., & Stillinger, F. H. (2001). Supercooled liquids and the glass transition. *Nature,*
551 410, 259.
552 Di Giacomo, R., Bonanomi, L., Costanza, V., Maresca, B., & Daraio, C. (2017). Biomimetic
553 temperature-sensing layer for artificial skins. *Science Robotics,* 2, 1-6.
554 Diaz, J. V., Anthon, G. E., & Barrett, D. M. (2007). Nonenzymatic Degradation of Citrus Pectin
555 and Pectate during Prolonged Heating: Effects of pH, Temperature, and Degree of Methyl
556 Esterification. *Journal of Agricultural and Food Chemistry,* 55, 5131-5136.
557 Einhorn-Stoll, U., Benthin, A., Zimathies, A., Görke, O., & Drusch, S. (2015). Pectin-water
558 interactions: Comparison of different analytical methods and influence of storage. *Food*
559 *Hydrocolloids,* 43, 577-583.
560 Einhorn-Stoll, U., Kastner, H., Urbisch, A., Kroh, L. W., & Drusch, S. (2018). Thermal
561 degradation of citrus pectin in low-moisture environment - Influence of acidic and alkaline
562 pre-treatment. *Food Hydrocolloids*.
563 Espitia, P. J. P., Du, W.-X., Avena-Bustillos, R. d. J., Soares, N. d. F. F., & McHugh, T. H.
564 (2014). Edible films from pectin: Physical-mechanical and antimicrobial properties - A
565 review. *Food Hydrocolloids,* 35, 287-296.
566 Fellah, A., Anjukandi, P., Waterland, M. R., & Williams, M. A. K. (2009). Determining the
567 degree of methylesterification of pectin by ATR/FT-IR: Methodology optimisation and
568 comparison with theoretical calculations. *Carbohydrate Polymers,* 78, 847-853.

569 Franco, C. R., Chagas, A. P., & Jorge, R. A. (2002). Ion-exchange equilibria with aluminum
570 pectinates. *Colloids and Surfaces A: Physicochemical and Engineering Aspects,* 204, 183-
571 192.
572 Hutchinson, J. M. (1995). Physical aging of polymers. *Progress in Polymer Science,* 20, 703-760.
573 Huynh, U. T. D., Lerbret, A., Neiers, F., Chambin, O., & Assifaoui, A. (2016). Binding of
574 Divalent Cations to Polygalacturonate: A Mechanism Driven by the Hydration Water. *The*
575 *Journal of Physical Chemistry B,* 120, 1021-1032.
576 Hwang, K. T., Kim, J. T., Jung, S. T., Cho, G. S., & Park, H. J. (2003). Properties of chitosan-
577 based biopolymer films with various degrees of deacetylation and molecular weights.
578 *Journal of Applied Polymer Science,* 89, 3476-3484.
579 Kpodo, F. M., Agbenorhevi, J. K., Alba, K., Bingham, R. J., Oduro, I. N., Morris, G. A., &
580 Kontogiorgos, V. (2017). Pectin isolation and characterization from six okra genotypes.
581 *Food Hydrocolloids,* 72, 323-330.
582 Kpodo, F. M., Agbenorhevi, J. K., Alba, K., Oduro, I. N., Morris, G. A., & Kontogiorgos, V.
583 (2018). Structure-Function Relationships in Pectin Emulsification. *Food Biophysics,* 13,
584 71-79.
585 Laurén, P., Paukkonen, H., Lipiäinen, T., Dong, Y., Oksanen, T., Räikkönen, H., . . . Laaksonen,
586 T. (2018). Pectin and Mucin Enhance the Bioadhesion of Drug Loaded Nanofibrillated
587 Cellulose Films. *Pharmaceutical Research,* 35, 145.
588 Lazaridou, A., & Biliaderis, C. G. (2002). Thermophysical properties of chitosan, chitosan–starch
589 and chitosan–pullulan films near the glass transition. *Carbohydrate Polymers,* 48, 179-190.
590 Lazaridou, A., Biliaderis, C. G., & Kontogiorgos, V. (2003). Molecular weight effects on
591 solutions rheology of pullulan and mechanical properties of its films. *Carbohydrate*
592 *Polymers,* 52, 151-166.
593 Li, X., Al-Assaf, S., Fang, Y., & Phillips, G. O. (2013). Characterisation of commercial LM-
594 pectin in aqueous solution. *Carbohydrate Polymers,* 92, 1133-1142.
595 Lins, L. C., Bugatti, V., Livi, S., & Gorrasi, G. (2018). Phosphonium ionic liquid as interfacial
596 agent of layered double hydroxide: Application to a pectin matrix. *Carbohydrate*
597 *Polymers,* 182, 142-148.
598 Makaremi, M., Pasbakhsh, P., Cavallaro, G., Lazzara, G., Aw, Y. K., Lee, S. M., & Milioto, S.
599 (2017). Effect of Morphology and Size of Halloysite Nanotubes on Functional Pectin
600 Bionanocomposites for Food Packaging Applications. *ACS Applied Materials &*
601 *Interfaces,* 9, 17476-17488.
602 Mohnen, D. (2008). Pectin structure and biosynthesis. *Current Opinion in Plant Biology,* 11, 266-
603 277.
604 Morris, E. R., Powell, D. A., Gidley, M. J., & Rees, D. A. (1982). Conformations and interactions
605 of pectins: I. Polymorphism between gel and solid states of calcium polygalacturonate.
606 *Journal of Molecular Biology,* 155, 507-516.
607 Nisar, T., Wang, Z.-C., Yang, X., Tian, Y., Iqbal, M., & Guo, Y. (2018). Characterization of citrus
608 pectin films integrated with clove bud essential oil: Physical, thermal, barrier, antioxidant
609 and antibacterial properties. *International journal of biological macromolecules,* 106, 670-
610 680.
611 Noreen, A., Nazli, Z.-i.-H., Akram, J., Rasul, I., Mansha, A., Yaqoob, N., . . . Zia, K. M. (2017).
612 Pectins functionalized biomaterials; a new viable approach for biomedical applications: A
613 review. *International Journal of Biological Macromolecules,* 101, 254-272.
614 Perron, P. J., & Lederman, P. B. (1972). The effect of molecular weight distribution on
615 polyethylene film properties. *Polymer Engineering and Science,* 12, 340-345.
616 Rinaudo, M. (2007). Main properties and current applications of some polysaccharides as
617 biomaterials. *Polymer International,* 57, 397-430.
618 Sperling, L. H. (2006). *Introduction to physical polymer science*. (4th ed.). New Jersey: John
619 Willet & Sons, Inc.

520 Ström, A., Ribelles, P., Lundin, L., Norton, I., Morris, E. R., & Williams, M. A. K. (2007).
521 Influence of Pectin Fine Structure on the Mechanical Properties of Calcium−Pectin and
522 Acid−Pectin Gels. *Biomacromolecules,* 8, 2668-2674.
523 Vieira, M. G. A., da Silva, M. A., dos Santos, L. O., & Beppu, M. M. (2011). Natural-based
524 plasticizers and biopolymer films: A review. *European Polymer Journal,* 47, 254-263.
525 Yoo, S.-H., Fishman, M. L., Hotchkiss, A. T., & Lee, H. G. (2006). Viscometric behavior of high-
526 methoxy and low-methoxy pectin solutions. *Food Hydrocolloids,* 20, 62-67.

527
528
529
530